Discrete-Time Signal Processing with DNA

Hua Jiang, Sayed Ahmad Salehi, Marc D. Riedel,* and Keshab K. Parhi

Department of Electrical Engineering, University of Minnesota, Minneapolis, Minnesota 55455, United States

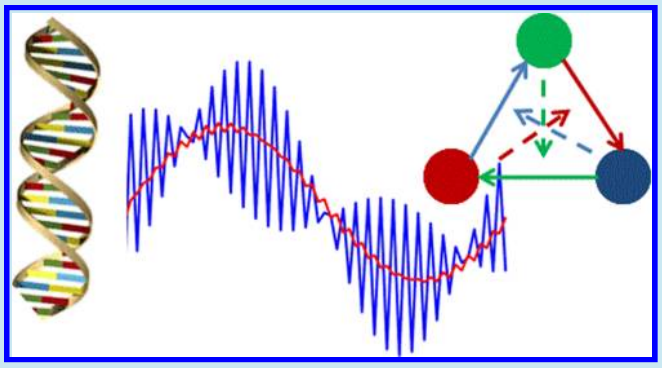

ABSTRACT: We present a methodology for implementing discrete-time signal processing operations, such as filtering, with molecular reactions. The reactions produce time-varying output quantities of molecules as a function of time-varying input quantities according to a functional specification. This computation is robust and independent of the reaction rates, provided that the rate constants fall within coarse categories. We describe two approaches: one entails synchronization with a clock signal, implemented through sustained chemical oscillations; the other is "self-timed" or asynchronous. We illustrate the methodology by synthesizing a simple moving-average filter, a biquad filter, and a Fast Fourier Transform (FFT). Abstract molecular reactions for these filters and transforms are translated into DNA strand displacement reactions. The computation is validated through mass-action simulations of the DNA kinetics. Although a proof of concept for the time being, molecular filters and transforms have potential applications in fields such as biochemical sensing and drug delivery.

KEYWORDS: *signal processing, molecular computing, DNA computing, DNA strand displacement, sequential circuits, recurrent circuits*

Electronic systems performing computation are pervasive in our modern lives. In addition to general-purpose computers, we have all manner of embedded controllers in our machines and gadgets. Electronic interfacing with biological systems is common, for instance, in biomedical devices. Such interfacing permits computational processing of biological data and actuation of responses, for instance, targeted drug delivery.

In some situations, one might want to implement computation directly *with* biological mechanisms. For example, one might want to implement a molecular mechanism for detecting protein markers of cancer and producing drugs targeted precisely to cancerous cells.[1,2] This could be achieved through genetic engineering, using bacterial or viral delivery systems. In essence, this approach is analogous to implementing embedded controllers with purely biological components.

Whereas electronic systems perform computation in terms of voltage, i.e., *energy per unit charge*, one can design molecular systems to perform computation in terms of molecular concentrations, i.e., *molecules per unit volume*. A particularly promising strategy for such computation is based on the mechanism of DNA strand displacement.[3,4]

The past few decades have seen a remarkable progress in the design of integrated circuits for signal processing for applications such as audio and video.[5] In abstract terms, signal processing circuits are *input-output* systems that transform given time-varying input signals into desired time-varying output signals. By interconnecting a few basic building blocks, namely, multipliers, adder, and delay units, complex signal processing systems can be synthesized. Signal processing operations are either "discrete-time" meaning that values are sampled and produced at specific points in time or "continuous-time" meaning that inputs are continuously transformed into outputs.

In this paper we present a methodology for implementing discrete-time signal processing operations with molecular reactions. We present two different frameworks: (1) a *synchronous* approach that transfers concentrations based on a molecular clock, and (2) a "self-timed" or *asynchronous* approach that transfers concentrations between molecular types based on the absence of other types. We illustrate our methodology with the design of a moving-average filter, a biquad filter, and an 8-point Fast Fourier Transform (FFT). We present both synchronous and asynchronous versions of each of these constructs.

For clarity, the methodology is first presented in terms of abstract molecular types; then a mapping to DNA strand displacement reactions is discussed. Critical for mapping to DNA, all of our designs consist of bimolecular reactions, that is to say, reactions with exactly two reactant molecules. In the mapping to DNA, we use experimental parameters similar to those of Soloveichik et al.[4] We generate differential equations corresponding to the mass-action chemical kinetics of the DNA reactions and simulate these to characterize the behavior of the designs. Such simulations of the chemical kinetics provide a reasonably accurate prediction of the actual *in vitro* behavior.

Special Issue: IWBDA 2012

Received: September 17, 2012

A molecular system consists of a set of chemical reactions, each specifying a rule for how different types of molecules combine. For instance,

$$X_1 + X_2 \xrightarrow{k} X_3$$

specifies that one molecule of X_1 combines with one molecule of X_2 to produce one molecule of X_3 at the rate k, referred to as the *rate constant*. If these molecular dynamics are represented in terms of *mass-action kinetics*, then the reaction rates are proportional to the concentrations of the participating molecular types and to the rate constant. Accordingly, for the above reaction, the rate of change in the concentrations of X_1, X_2, and X_3 is given by

$$-\frac{d[X_1]}{dt} = -\frac{d[X_2]}{dt} = \frac{d[X_3]}{dt} = k[X_1][X_2] \quad (1)$$

where $[X]$ denotes the concentration of the entity X. Such a differential equation representation suggests immediate parallels with the systems developed in the field of electrical engineering.

Most prior schemes for molecular computation depend on specific values of the rate constants, which limits the applicability since the rate constants are not constant at all; they depend on factors such as cell volume and temperature. Accordingly, the results of the computation are not robust. We aim for robust constructs: in our methodology we require only two coarse rate categories for the rate constants, i.e., k_{fast} and k_{slow}. Given reactions with any such set of rates, the computation is exact. It does not matter how fast the "fast" reactions are or how slow the "slow" reactions are — only that all fast reactions fire relatively faster than slow reactions.

METHODOLOGY

We present two frameworks for discrete-time signal processing. The first is a synchronous framework; the second is a "self-timed" or asynchronous framework. We will first illustrate both schemes with a simple example, a moving-average filter.

The circuit diagram for the filter is shown in Figure 1. It produces an output value that is one-half the current input value plus one-half the previous value. Given a time-varying input signal X, the output signal Y is a moving average, i.e., a smoother version of the input signal. Since there is no feedback in the system, it is called a *finite impulse response* (FIR) filter.[5]

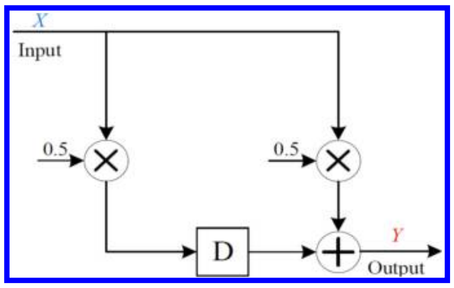

Figure 1. Circuit diagram for the moving-average filter.

a. Synchronous Framework. The synchronous framework is illustrated in general terms in Figure 2. As in an electronic system, this molecular system has separate constructs for *computation* and for *memory*. A clock signal synchronizes transfers signals between the two. Here we give a simplified description of these mechanisms pertaining to the moving-average filter. Molecular reactions for generating the clock signal, for the memory constructs, and for the computational constructs are described in detail in later sections.

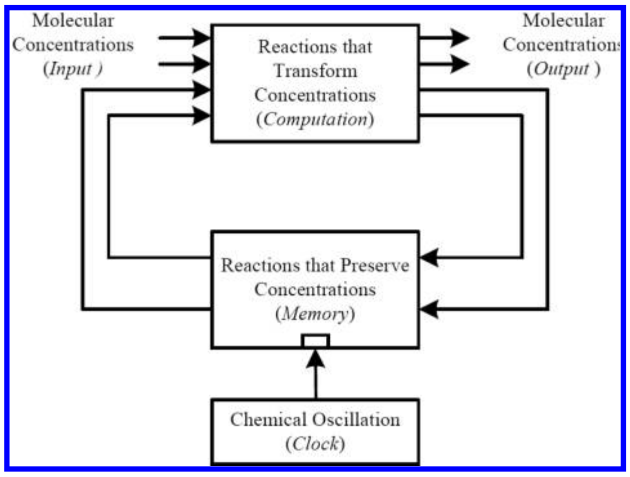
Molecular Concentrations (Input)
Molecular Concentrations (Output)
Reactions that Transform Concentrations (Computation)
Reactions that Preserve Concentrations (Memory)
Chemical Oscillation (Clock)
Figure 2. Synchronous framework.

The delay and computation elements for the moving average filter in Figure 3 are implemented by the reactions in Figure 4.

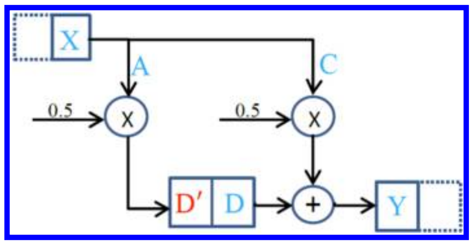

Figure 3. Synchronous implementation of the moving-average filter.

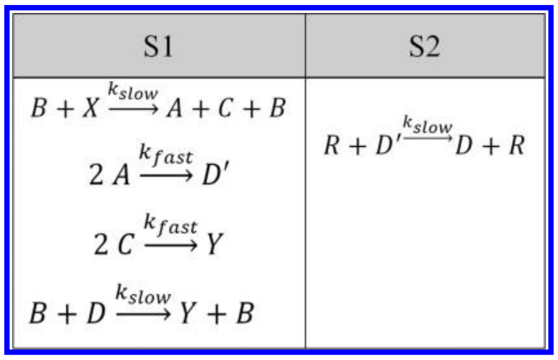

S1	S2
$B + X \xrightarrow{k_{slow}} A + C + B$	$R + D' \xrightarrow{k_{slow}} D + R$
$2\,A \xrightarrow{k_{fast}} D'$	
$2\,C \xrightarrow{k_{fast}} Y$	
$B + D \xrightarrow{k_{slow}} Y + B$	

Figure 4. Set of molecular reactions for the synchronous implementation of the moving-average filter.

We assume that a two-phase clock generates and consumes the molecular types R and B in alternating fashion. In the presence of B, the input signal X is transferred to molecular types A and C; these are both reduced to half and transferred to D' and Y, respectively. In the presence of R, D' is transferred to D. Details regarding how the clock signals R and B are generated are given in a later section.

b. Asynchronous Framework. The asynchronous framework is illustrated in Figure 5. It contains no clock signal; rather it is "self-timed" in the sense that a new phase of the computation begins when an external sink removes the entire quantity of molecules Y, i.e., the previous output value, and

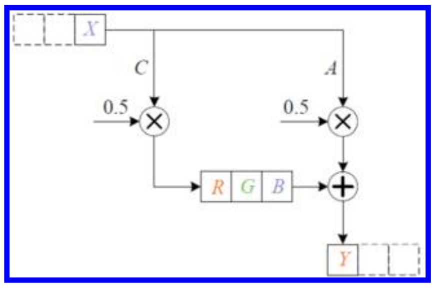

Figure 5. Aynchronous implementation of the moving-average filter.

supplies a new quantity of molecules X, i.e., the current input value.

In this framework, the moving-average filter is implemented by the reactions in Figure 6. The molecular types corresponding to *signals* are X, A, C, R, G, B, and Y. To illustrate the design, we use colors to categorize some of these types into three categories: Y and R in red; G in green; and X and B in blue. The group of the first three reactions shown in the S1 column of Figure 6 transfers the concentration of X to A and to C, a *fanout* operation. The concentrations of A and C are both reduced to half, *scalar multiplication* operations. The concentration of A is transferred to the output Y, and the concentration of C is transferred to R. The transfer to R is the first phase of a *delay* operation. Once the signal has moved through the delay operation, the concentration of B is transferred to the output Y. Since this concentration is combined with the concentration of Y produced from A, this is an *addition* operation.

The final group of three reactions shown in the S1 column of Figure 6 implements the delay operation. The concentration of R is transferred to G and then to B. Transfers between two color categories are enabled by the absence of the third category: red goes to green in the absence of blue; green goes to blue in the absence of red; and blue goes to red in the absence of green. The reactions are enabled by molecular types r, g, and b that we call *absence indicators*. The absence indicators ensure that the delay element takes a new value only when it has finished processing the previous value.

In the group of reactions shown in the S2 column of Figure 6 molecules of types R', G', and B' are generated from the signal types that we color-code red, green, and blue, respectively. The concentrations of the signal types remain unchanged. (These reactions appear to violate conservation of mass. In fact, when mapped to DNA reactions, there are external "fuel" types.) Meanwhile, R', G', and B' are consumed by external sinks, denoted by $\varnothing$. When mapped to DNA, these reactions produce the "waste" types. Here, all reactions are expressly designed to have two reactants; this permits us to map the reactions to DNA strand displacement reactions effectively. This generation/consumption process ensures that equilibria of the concentrations of R', G', and B' reflect the total concentrations of red, green, and blue color-coded types, respectively. Accordingly, we call R', G', and B' *color concentration indicators*. They serve to speed up signal transfers between color categories.

In the group of reactions shown in the S3 column of Figure 6, molecules of the absence indicator types r, g, and b are generated from external sources S_r, S_g, and S_b. At the same time, they are consumed when R', G', and B' are present, respectively. Therefore, the absence indicators only persist in the absence of the corresponding signals: r in the absence of red types; g in the absence of green types; and b in the absence of blue types. They only persist in the absence of these types because otherwise "fast" reactions consume them quickly.

Finally, the group of reactions shown in the S4 column of Figure 6 provides positive feedback kinetics. These reactions effectively speed up transfers between color categories as molecules in one category are "pulled" to the next by color concentration indicators. Note that the concentration of the input X is sampled in the green-to-blue phase. We assume that an external source supplies the input. The output Y is produced in the blue-to-red phase. We assume that an external sink consumes these molecules.

Clock. In electronic circuits, a clock signal is generated by an oscillatory circuit that produces periodic voltage pulses. For a molecular clock, we choose reactions that produce sustained oscillations in terms of chemical concentrations. With such oscillations, a low concentration corresponds to a logical value of zero; a high concentration corresponds to a logical value of one.

Techniques for generating chemical oscillations are well established in the literature. Classic examples include the Lotka-Volterra, the "Brusselator", and the Arsenite-Iodate-Chlorite systems.[6,7] Unfortunately, none of these schemes are quite

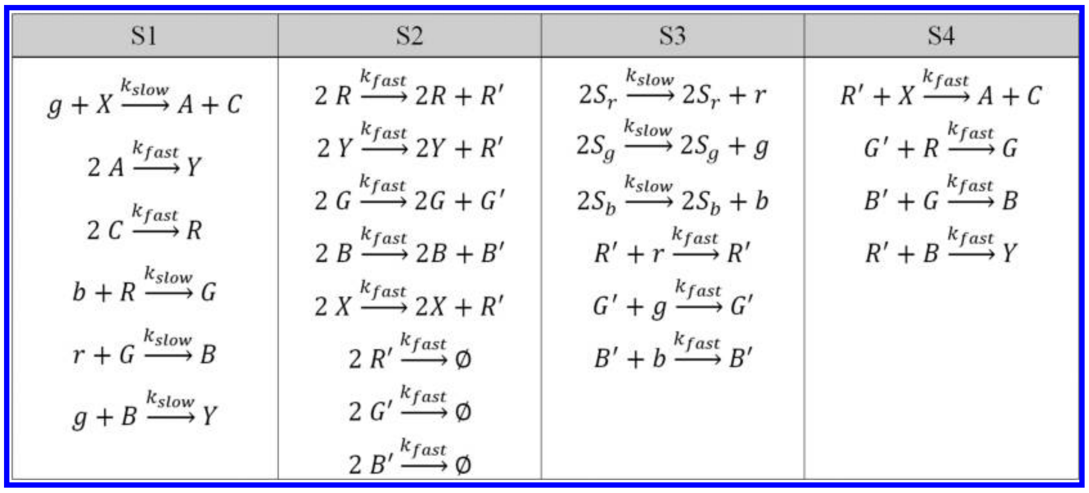

S1	S2	S3	S4
$g + X \xrightarrow{k_{slow}} A + C$	$2\,R \xrightarrow{k_{fast}} 2R + R'$	$2S_r \xrightarrow{k_{slow}} 2S_r + r$	$R' + X \xrightarrow{k_{fast}} A + C$
$2\,A \xrightarrow{k_{fast}} Y$	$2\,Y \xrightarrow{k_{fast}} 2Y + R'$	$2S_g \xrightarrow{k_{slow}} 2S_g + g$	$G' + R \xrightarrow{k_{fast}} G$
$2\,C \xrightarrow{k_{fast}} R$	$2\,G \xrightarrow{k_{fast}} 2G + G'$	$2S_b \xrightarrow{k_{slow}} 2S_b + b$	$B' + G \xrightarrow{k_{fast}} B$
$b + R \xrightarrow{k_{slow}} G$	$2\,B \xrightarrow{k_{fast}} 2B + B'$	$R' + r \xrightarrow{k_{fast}} R'$	$R' + B \xrightarrow{k_{fast}} Y$
$r + G \xrightarrow{k_{slow}} B$	$2\,X \xrightarrow{k_{fast}} 2X + R'$	$G' + g \xrightarrow{k_{fast}} G'$	
$g + B \xrightarrow{k_{slow}} Y$	$2\,R' \xrightarrow{k_{fast}} \varnothing$	$B' + b \xrightarrow{k_{fast}} B'$	
	$2\,G' \xrightarrow{k_{fast}} \varnothing$		
	$2\,B' \xrightarrow{k_{fast}} \varnothing$		

Figure 6. Set of molecular reactions for the asynchronous implementation of the moving-average filter.

suitable for synchronous sequential computation: we require that the clock signal be symmetrical, with abrupt transitions between the phases. Here, we present a new design for an n-phase chemical oscillator ($n \geq 3$). The clock phases are represented by molecular types $P_1, P_2, ..., P_n$. First consider the reactions

$$2S_1 \xrightarrow{k_{\text{slow}}} a_1 + 2S_1,\ 2S_2 \xrightarrow{k_{\text{slow}}} a_2 + 2S_2,\ ...,\ 2S_n \xrightarrow{k_{\text{slow}}} a_n + 2S_n \quad (3)$$

$$P_1 + a_1 \xrightarrow{k_{\text{fast}}} P_1,\ \ P_2 + a_2 \xrightarrow{k_{\text{fast}}} P_2,\ ...,\ P_n + a_n \xrightarrow{k_{\text{fast}}} P_n \quad (4)$$

In reactions 3, the molecular types $a_1, a_2, ..., a_n$ are generated slowly and constantly, from source types $S_1, S_2, ..., S_n$, whose concentrations do not change with the reactions. Here, all reactions are expressly designed to have two reactants; as discussed above, this permits us to map the reaction to DNA strand displacement reactions effectively.

In reactions 4, the types $P_1, P_2, ..., P_n$ quickly consume the types $a_1, a_2, ..., a_n$, respectively. Call $P_1, P_2, ..., P_n$ the *phase signals* and $a_1, a_2, ..., a_n$ the *absence indicators*. The latter are only present in the absence of the former. The reactions

$$P_1 + a_n \xrightarrow{k_{\text{slow}}} P_2,\ P_2 + a_1 \xrightarrow{k_{\text{slow}}} P_3,\ ...,\ P_n + a_{n-1} \xrightarrow{k_{\text{slow}}} P_1 \quad (5)$$

transfer one phase signal to another, in the absence of the previous one. The essential aspect is that, within the $P_1, P_2, ..., P_n$ sequence, the full quantity of the preceding type is transferred to the current type before the transfer to the succeeding type begins. To achieve sustained oscillation, we introduce positive feedback. This is provided by the reactions

$$\begin{gathered}
2P_1 \xrightarrow{k_{\text{slow}}} I_1,\ 2I_1 \xrightarrow{k_{\text{fast}}} 4P_1,\ P_n + I_1 \xrightarrow{k_{\text{fast}}} 3P_1 \\
2P_2 \xrightarrow{k_{\text{slow}}} I_2,\ 2I_2 \xrightarrow{k_{\text{fast}}} 4P_2,\ P_1 + I_2 \xrightarrow{k_{\text{fast}}} 3P_2 \\
\vdots \\
2P_n \xrightarrow{k_{\text{slow}}} I_n,\ 2I_n \xrightarrow{k_{\text{fast}}} 4P_n,\ P_{n-1} + I_n \xrightarrow{k_{\text{fast}}} 3P_n
\end{gathered} \quad (6)$$

Consider the first three reactions. Two molecules of P_1 combine with one molecule of P_n to produce three molecules of P_1. The first step in this process is reversible: two molecules of P_1 can combine, but in the absence of any molecules of P_n, the combined form will dissociate back into P_1. So, in the absence of P_n, the quantity of P_1 will not change much. In the presence of P_n, the sequence of reactions will proceed, producing one molecule of P_1 for each molecule of P_n that is consumed. Due to the first reaction, the transfer will occur at a rate that is superlinear in the quantity of P_1; this speeds up the transfer and so provides positive feedback. Suppose that the initial quantity of P_1 is set to some non-zero amount, and the initial quantity of the other types is set to zero. We will get an oscillation among the quantities of $P_1, P_2, ..., P_n$.

One requirement for a clock in synchronous computation is that different clock phases should not overlap. In this paper we use a two-phase clock for synchronous structures: concentrations of molecular types representing clock phase "0" and clock phase "1" should not be present at the same time. To this end, we choose two nonadjacent phases, P_1 and P_3 in a four-phase oscillator, as the clock phases. For a clearer illustration, we use $R(ed)$ to denote P_1 and $B(lue)$ to denote P_3.

Our scheme for chemical oscillation works well. Figure 7 shows the concentrations of R and B as a function of time,

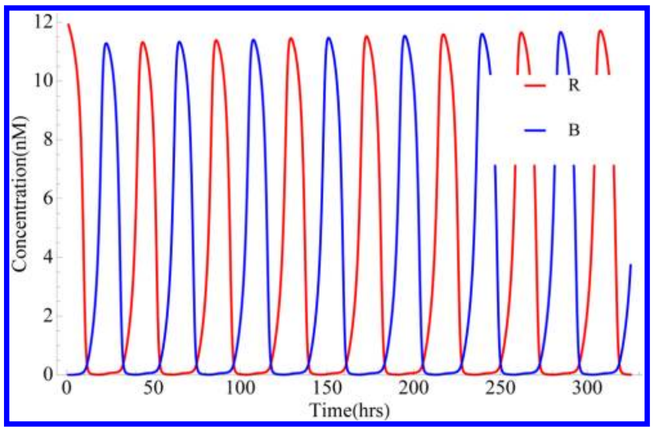

Figure 7. Differential equation simulation of the chemical kinetics of our proposed N-phase clock. In this simulation, N is set to 2. In principle, the amplitude and frequency of oscillations can be controlled.

obtained through differential equation simulations of the reactions 3, 4, 5 and 6. It may be noted that the two phases R and B are essentially non-overlapping.

DELAY ELEMENTS

a. Synchronous Delay Elements. To implement sequential computation, we must store and transfer signals across clock cycles. In electronic systems, storage is typically implemented with flip-flops. In our molecular system, we implement storage and transfer using a two-phase protocol, synchronized on phases of our clock. As Figure 8 illustrates,

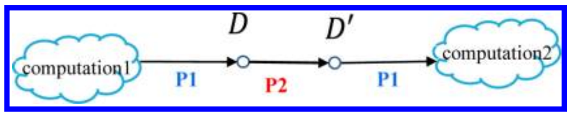

Figure 8. A delay element in the synchronous scheme.

every memory unit is assigned two molecular types D'_i and D_i. Here D'_i is the first stage and D_i the second. The blue phase reactions are

$$\begin{gathered}
B + D_i \xrightarrow{k_{\text{slow}}} \text{computations} + B \\
\text{computations} \xrightarrow{k_{\text{fast}}} D'_i
\end{gathered} \quad (7)$$

Every delay unit releases the signal it stores in its second stage D_i. The released signal is operated on by reactions in computational modules. These generate results and push them into the first stages of succeeding memory units. Note that D'_i molecules will be the first stage of any succeeding memory unit along the signal path. The red phase reactions are

$$R + D'_i \xrightarrow{k_{\text{slow}}} D_i + R \quad (8)$$

A delay unit transfers the signal it stores in D'_i to D_i, preparing for the next cycle. It is the equivalent of a *delay (D) flip-flop* in an electronic system.

b. Asynchronous Delay Elements. In our asynchronous scheme, we implement delay elements by transferring concentrations between molecular types based on the absence of other types. Each delay element DE_i is assigned three molecular types $R(ed)_i$, $G(reen)_i$ and $B(lue)_i$. Let b be an *absence indicator* for B. The element is implemented by the following reactions:

- **Phase 1** reactions: $b + R_i \xrightarrow{k_{\text{slow}}} G_i$, $G' + R_i \xrightarrow{k_{\text{fast}}} G_i$.
- **Phase 2** reactions: $b + G_i \xrightarrow{k_{\text{slow}}} B_i$, $B' + G_i \xrightarrow{k_{\text{fast}}} B_i$.
- **Phase 3** reactions: $g + B_i \xrightarrow{k_{\text{slow}}}$ computations, $R' + B_i \xrightarrow{k_{\text{fast}}}$ computations.

A computation cycle, in which an input value is accepted and an output value is computed, completes in three phases. The input X is injected in phase 2 and the output Y is collect in phase 1. In each phase the signals are transferred from molecular types in one color category to the next. Computations, including scalar multiplication, addition, and fanout, are carried out in phase 3, during the transfer from blue to red:

$$\text{computations} \xrightarrow{k_{\text{fast}}} R_j$$

This is illustrated in Figure 9(i).

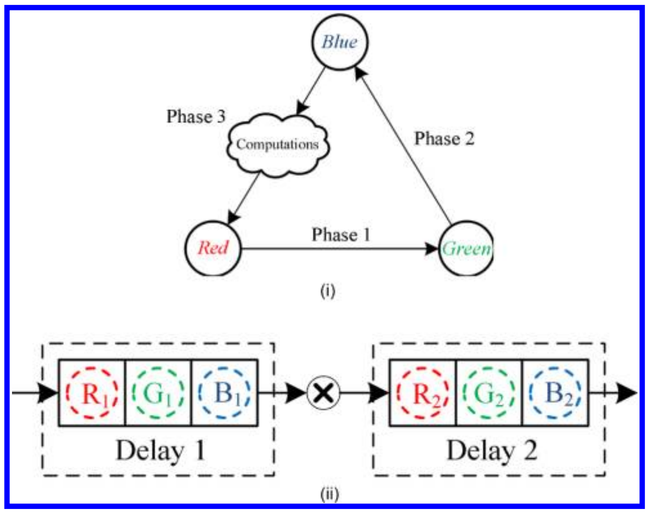

Figure 9. (i) Implementing delay elements using the 3-phase asynchronous scheme. (ii) Cascaded delay elements implemented using the asynchronous scheme.

We use the notation $Delay(R_i,G_i,B_i,\{output\_list\})$ to represent the above three reactions. Here, $\{output\_list\}$ is a list of molecular types that B_i should be transferred to during phase 3. The input X is labeled blue, therefore, reactions

$$g + X \xrightarrow{k_{\text{slow}}} \text{computations}, \quad R' + X \xrightarrow{k_{\text{fast}}} \text{computations}$$

also fire in phase 3. We use $Input(X,\{output\_list\})$ to represent these reactions.

The computation reactions fire much faster than the transfer reactions, so molecules of R_j are immediately produced from molecules of B_i. Thus, reactions in phase 3 effectively transfer blue signals to red signals. Note that R_j produced in phase 3 will be a red type of any succeeding delay element DE_j along the signal path from DE_i. In Figure 9ii, R_1 and R_2 are red; G_1 and G_2 are green; B_1 and B_2 are blue. The multiplier is the computation that occurs between the delay elements. DE_2 is a succeeding delay element of DE_1, so molecules of B_1 are transferred to R_2 in phase 3. For each delay element, the color concentration types R', G', and B' are generated and consumed in the following reactions:

$$2R_i \xrightarrow{k_{\text{fast}}} 2R_i + R', \ 2Y \xrightarrow{k_{\text{fast}}} 2Y + R', \ 2G_i \xrightarrow{k_{\text{fast}}} 2G_i + G', \ 2B_i \xrightarrow{k_{\text{fast}}} 2B_i + B', \ 2X \xrightarrow{k_{\text{fast}}} 2X + B', \ 2R' \xrightarrow{k_{\text{fast}}} \varnothing, \ 2G' \xrightarrow{k_{\text{fast}}} \varnothing, \ 2B' \xrightarrow{k_{\text{fast}}} \varnothing \quad (9)$$

So molecules of R', G', and B' are generated by types of the corresponding color categories; they are consumed by external sinks. The equilibrium levels of these three types are determined by total concentrations of all the red types, blue types, and green types, respectively. Note that these reactions are in the "fast" category, since the color concentration types cannot lag the signal types. We use $Conc(R',\{red\_type\_list\})$, $Conc(G',\{green\_type\_list\})$, $(B',\{blue\_type\_list\})$ to represent Reactions 9. For example, $Conc(R',\{R_1,Y\})$ represents $2R_1 \xrightarrow{k_{\text{fast}}} 2R_1 + R'$, $2Y \xrightarrow{k_{\text{fast}}} 2Y + R'$, $2R' \xrightarrow{k_{\text{fast}}} \varnothing$. For delay elements, the following reactions generate the absence indicator types r, g, and b:

$$2S_r \xrightarrow{k_{\text{slow}}} 2S_r + r, \ R' + r \xrightarrow{k_{\text{fast}}} R', \ 2S_g \xrightarrow{k_{\text{slow}}} 2S_g + g, \ G' + g \xrightarrow{k_{\text{fast}}} G', \ 2S_b \xrightarrow{k_{\text{slow}}} 2S_b + b, \ B' + b \xrightarrow{k_{\text{fast}}} B' \quad (10)$$

We use the notation $Abs(S_r,S_g,S_b,r,g,b,R',G',B')$ to represent these reactions. Here r, g, and b are continually and slowly generated. However, they persist only in the absence of the corresponding color-coded types, since they are quickly consumed by R', G', and B', respectively, if these are present. All transfers are initiated by absence indicators and then sped up by the color concentration indicators. The transfers initiated by the absence indicators are slow, and those initiated by the color concentration indicators are fast. This mitigates against "leakage", e.g., some transferring from G_i to B_i before all of transferring from R_i to G_i is complete.

Note that, in any system, there are only three color concentration indicators (R', G', and B') and three absence indicators (r, g, and b), regardless of the number of delay elements. These types help enable and speed up signal transfers for all reactions in the corresponding color categories. Through these common indicators, the corresponding phases of all delay elements are synchronized: all of the delay elements must wait for each to complete its current phase before they can move to the next phase.

COMPUTATIONS

General signal processing operations can be specified in terms of three basic modules: scalar multiplication, addition, and delay elements. Above, we discussed delay elements in detail. Scalar multiplication and addition are much simpler.

Scalar multiplication performs the operation

$$y = \frac{c_2}{c_1}x$$

where c_1 and c_2 are constants. This operation is implemented by choosing reactions with the appropriate coefficients:

$$c_1X \rightarrow c_2Y$$

Every time this reaction fires, c_1 molecules of X get transferred to c_2 molecules of Y. Once the reaction has fired to completion, i.e., fully consumed all molecules of X, the requisite operation of scalar multiplication is complete.

Addition performs the operation $y = x1 + x2$. This operation is implemented by choosing two or more reactions with the same product:

$$2X_1 \xrightarrow{k_{\text{fast}}} 2Y$$
$$2X_2 \xrightarrow{k_{\text{fast}}} 2Y$$

For implementation with DNA, we choose bimolecular reactions instead of unimolecular transfers, such as $X_1 \xrightarrow{k_{\text{fast}}} Y$. Once both of these reactions have fired to completion, the concentration of Y will be the former concentration of X_1 plus the former concentration of X_2. It should be noted that implementations of multiplication and addition are the same in the synchronous and asynchronous schemes.

BIQUAD FILTER

We illustrate the general design method with a second detailed example, a biquad filter. The circuit diagram for the filter is shown in Figure 10i. Since this design has feedback, it is called an infinite impulse response (IIR) filter. Biquad filters are basic building blocks of modern signal processing systems. Highly stable, high-order filters can be implemented by cascaded biquad blocks.[5]

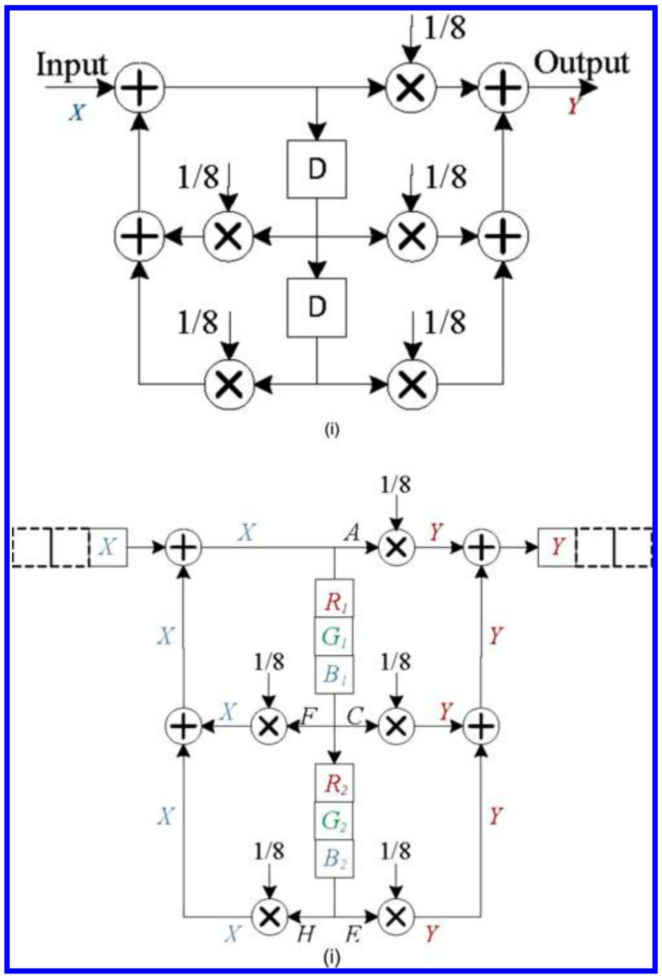

Figure 10. (i) Circuit diagram of a biquad filter. (ii) A biquad filter in a 3-phase asynchronous configuration.

a. Synchronous Biquad Filter. The following reactions provide a synchronous implementation of the biquad filter.

$$\begin{aligned} B + X &\xrightarrow{k_{\text{slow}}} B + A + D'_1 \\ B + D_1 &\xrightarrow{k_{\text{slow}}} B + F + C + D'_2 \\ B + D_2 &\xrightarrow{k_{\text{slow}}} B + H + E \end{aligned} \quad (11)$$

$$\begin{aligned} &2A \xrightarrow{k_{\text{fast}}} A_2,\ 2A_2 \xrightarrow{k_{\text{fast}}} A_4,\ 2A_4 \xrightarrow{k_{\text{fast}}} Y, \\ &2C \xrightarrow{k_{\text{fast}}} C_2,\ 2C_2 \xrightarrow{k_{\text{fast}}} C_4,\ 2C_4 \xrightarrow{k_{\text{fast}}} Y, \\ &2E \xrightarrow{k_{\text{fast}}} E_2,\ 2E_2 \xrightarrow{k_{\text{fast}}} E_4,\ 2E_4 \xrightarrow{k_{\text{fast}}} Y, \\ &2F \xrightarrow{k_{\text{fast}}} F_2,\ 2F_2 \xrightarrow{k_{\text{fast}}} F_4,\ 2F_4 \xrightarrow{k_{\text{fast}}} X, \\ &2H \xrightarrow{k_{\text{fast}}} H_2,\ 2H_2 \xrightarrow{k_{\text{fast}}} H_4,\ 2H_4 \xrightarrow{k_{\text{fast}}} X \end{aligned} \quad (12)$$

$$\begin{aligned} R + D'_1 &\xrightarrow{k_{\text{slow}}} R + D_1 \\ R + D'_2 &\xrightarrow{k_{\text{slow}}} R + D'_2 \end{aligned} \quad (13)$$

In the set of reactions 11, with clock phase B, signal X is transferred to A and D'_1 ; D_1 is transferred to C, F and D'_2 ; D_2 is transferred to H and E. In the set of reactions 12, temporary signals A, C, E, F and H are multiplied by $(1/8)$ and transferred to either X or Y. In the set of reactions 13, with clock phase R, signal transfers inside memory units take place.

b. Asynchronous Biquad Filter. An asynchronous implementation of the biquad filter is shown in in Figure 10ii. It is realized by the following reactions:

- Delay elements: $Delay(R_1,G_1,B_1,\{R2,F,C\})$, $Delay(R_2,G_2,B_2,\{H,E\})$.
- System input: $Input(X,\{R_1,A\})$.
- Scalar multiplications: $Mult(A,Y,8,1),(C,Y,8,1),(E,Y,8,1),(F,X,8,1),(H,X,8,1)$.
- Concentration indicators: $Conc(R',\{R1,R2,Y\})$, $Conc(G',\{G1,G2\})$, $Conc(B',\{B1,B2,X\})$.
- Absence indicators: $Abs(S_r,S_g,S_b,r,g,b,R',G',B')$.

8-POINT RFFT

The N-point Discrete Fourier Transfer (DFT)[8] is defined mathematically as

$$X[k] = \sum_{n=0}^{N-1} x(n)\, e^{-i2k\pi n/N} \qquad k = 0,\ 1,\ \ldots,\ N-1 \quad (14)$$

(here i is the imaginary unit).

The DFT represents decomposition of a sequence of values $x(n)$ into components of different frequencies, $X[k]$. In essence, it transforms a signal from the time domain to the *spectral* or frequency domain. Such a transform is useful for a wide variety of applications; indeed, it is ubiquitous in communication systems.

The so-called Fast Fourier Transform (FFT) algorithm is a computationally less expensive alternative to the DFT. In the FFT, the input sequence is first divided to two subsequences: the even and odd indexed samples. Replacing the original sequence by a sum of such shorter sequences simplifies the transform. Repeating this, the entire transform can be converted to a set of 2-point DFT elements called "butterfly" (BF) units. A BF unit is shown in Figure 13i.

It is easy to show that for real valued signals, we have

$$X[k] = X^*[N - k] \quad (15)$$

So it is not necessary to compute all of the FFT coefficients. By eliminating the computations of $((N/2) - 1)$ conjugate-symmetric outputs and separating them into real and imaginary parts, one obtains the structure shown in Figure 11, called a *real-valued* FFT (RFFT).

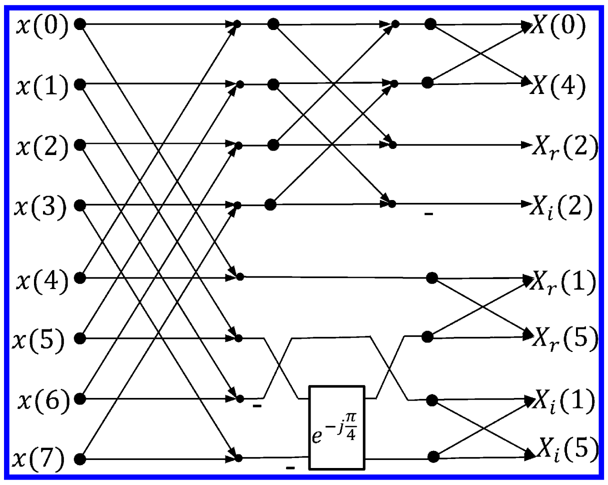

Figure 11. RFFT for 8-point sequence $x(n)$. X_r and X_i represent real and imaginary parts of the output, respectively.

Using folding methods,[5] this structure can be mapped to the 4-parallel pipelined architecture shown Figure 12. I_1, I_2, I_3, and I_4 sample $x(0)$, $x(1)$, $x(2)$, and $x(3)$, in the first clock cycle, and $x(4)$, $x(5)$, $x(6)$, and $x(7)$ in the second cycle, respectively. We describe how this architecture can be realized by molecular reactions.

The structure shown in Figure 12 consists of BFs, multipliers, and multiplexers. These operations and the corresponding molecular reactions are shown in Figure 13. We need to estimate multiplication by $\sqrt{2}$. Because $\sqrt{2} \simeq 1+ (1/4) + (1/8)$, multiplication by $\sqrt{2}$ can be implemented as shown in Figure 13ii. Activation for control signals of multiplexer, S1 and S2, should alternatively be toggled for every new input set. In the synchronous scheme, activation of S1 and S2 toggles in phase *B* of the clock, whereas in the asynchronous scheme, it toggles in *G* phase.

The RFFT architecture is implemented using computation modules and delay units, as well as the elements shown in Figure 13. Because concentration of a molecular type cannot be negative, we use one molecular type for positive and another one for negative part of each signal. Finally these two parts cancel out each other, and the one that has larger concentration determines the sign of that signal. For example, if x_p and x_n represent positive and negative part of signal x, then the following reactions performs the positive/negative cancellation:

$$x_p + x_n \xrightarrow{k_{\text{fast}}} \varnothing \quad (16)$$

(Here ∅ denotes a waste product that we do not track.) For simplicity, in Figure 13 we present only reactions related to positive part. The reactions for negative part are analogous.

SIMULATION RESULTS

Mapping to DNA Strand Displacement. Given a specification of an abstract set of molecular reactions that implements the requisite computation, the next step is to map it to specific molecular reactions. We describe a mapping to DNA strand displacement reactions. The reader is referred to Soloveichik et al. for a detailed discussion of this mechanism.[4] The following is a simple example.

Consider the DNA strand displacement reaction shown in Figure 14. Here a single strand of DNA R_1 replaces the top strand of a double-strand DNA *L*; this generates a double strand *H* and a single strand *B*. (This reaction is reversible.) One of the top strands of the double strand *H* can be replaced by a single strand R_2, generating a single strand *O*. Then *O* replaces the top strand of *T*, releasing *P*. (Note that the strands *L*, *G*, and *T* are "fuel" sources. It is assumed that there is an abundant source of these; the concentrations do not matter.) The signals are the concentrations of R_1, R_2, and *P*. This sequence of strand displacements implements the abstract chemical reaction: $R_1 + R_2 \xrightarrow{k} P$.

Simulation Results. To validate our designs for moving-average filter, the biquad filter, and the Fast Fourier Transform, we map their bimolecular reactions to DNA strand displacement reactions, using the method discussed in Soloveichik et al.[4] We generate the corresponding system of kinetic differential equations using similar parameters to Soloveichik et al. We simulate the differential equations to characterize the behavior of the system.

The initial concentrations of auxiliary complexes is set to $C_{\text{max}} = 10^{-5}$ M, and the maximum strand displacement rate constant is $q_{\text{max}} = 10^6$ M^{-1} s^{-1}. The rate constant for the "slow" reactions is set to $k_{\text{slow}} = 5.56 \times 10^4$ M^{-1} s^{-1}. For "fast"

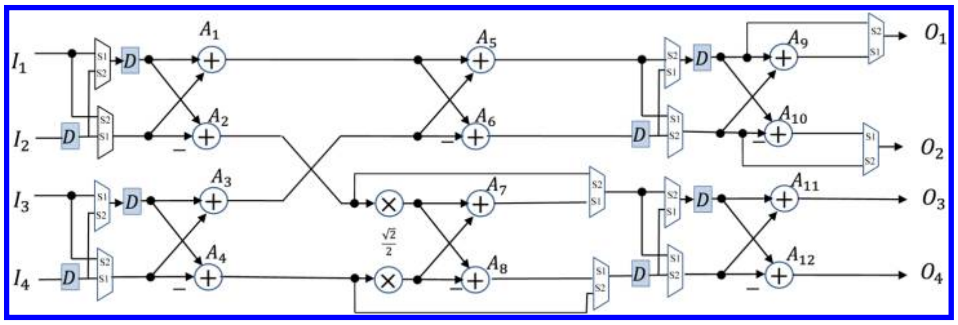

Figure 12. Folded 8-point 4-parallel RFFT.

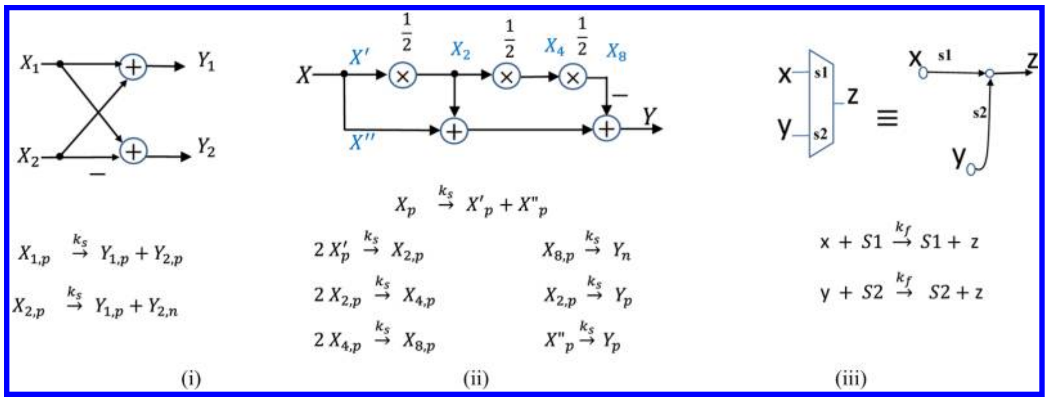

Figure 13. Abstract molecular reactions for different elements in Figure 12: (i) BF; (ii) multiplication by $\sqrt{2}$; (iii) multiplexer.

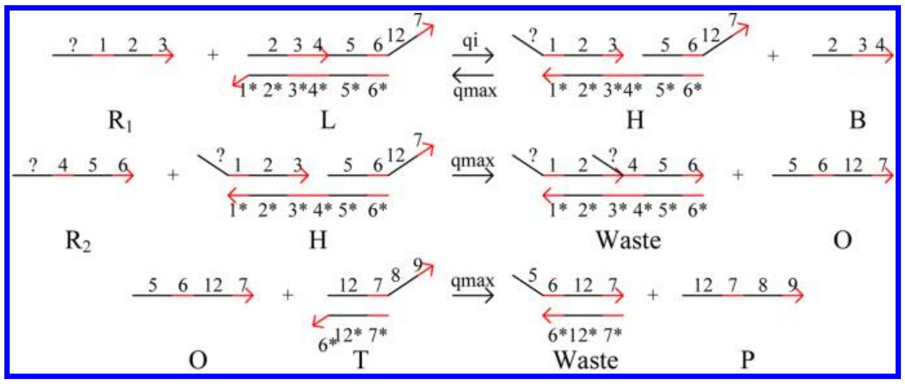

Figure 14. Example of DNA strand displacement.

reactions it is set to $k_{fast} = 3 \times k_{slow}$. The initial concentrations of S_r, S_g, and S_b are set to 1 nM.

The simulation results for the synchronous and asynchronous moving-average filters are shown in Figures 15 and 16, respectively. The input is a time-varying signal concentration X with both high-frequency and low-frequency components. The output is a time-varying signal concentration Y. Molecules of X are injected and molecules of Y are collected from the systems every 72 h for the synchronous scheme and every 20 h for the asynchronous scheme. The figure shows the theoretical output, i.e., an exact calculation of filtering, as well as simulation results. We see that our design performs very well, filtering out the high-frequency component as expected.

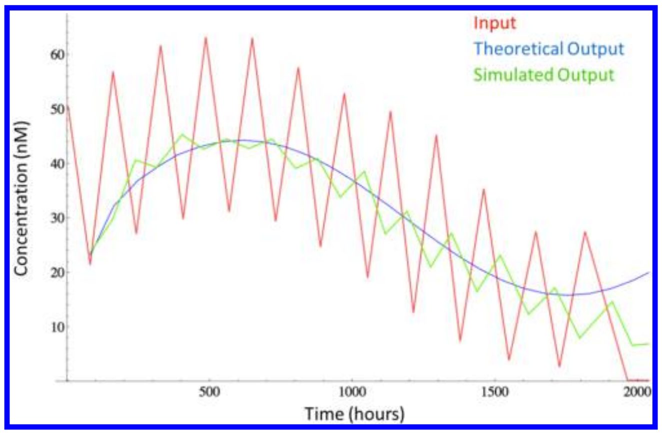

Figure 15. Simulation results for the DNA implementation of the synchronous moving average filter.

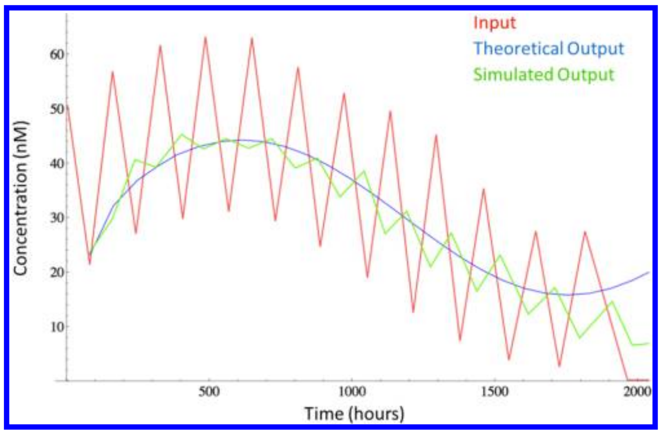

Figure 16. Simulation results for the DNA implementation of the asynchronous moving average filter.

The simulation results for the synchronous an asynchronous biquad filters are shown in Figures 17 and 18, respectively. Here, molecules of X are injected and molecules of Y are collected from the synchronous and asynchronous scheme systems every 70 and 50 h, respectively. We supply step-like and impulse-like changes in X. The figure shows the theoretical output, i.e., an exact calculation of filtering, as well as simulation results. As expected, the system performs "notch" filtering.[5] The simulation results show that even for a ratio $\lambda = k_{fast}/k_{slow}$ as low as 3, the systems perform well. In fact, in experimental implementations of DNA strand displacement systems, a ratio λ greater than 1000 is readily achievable. When λ is close to 1, i.e., fast reactions are not much faster than slow reactions, the concentrations of the absence indicators r, g, and b are high

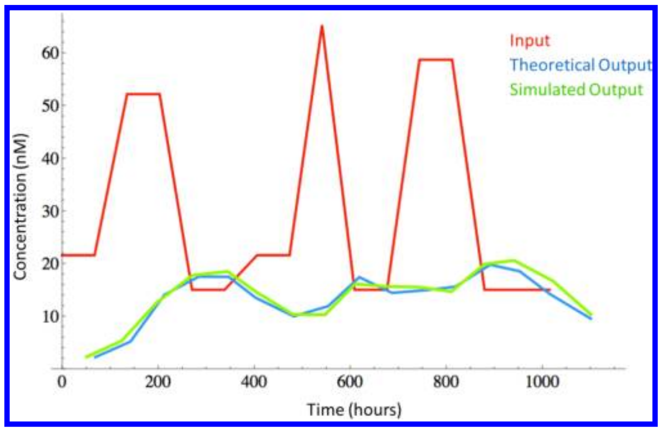

Figure 17. Simulation results for the DNA implementation of the synchronous biquad filter.

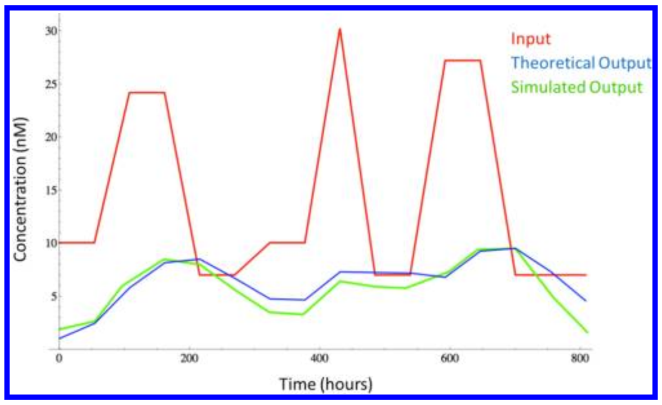

Figure 18. Simulation results for the DNA implementation of the asynchronous biquad filter.

even when the concentrations of R', G', or B' are high. Also, the computational modules slow down. Accordingly, the accuracy of the computation degrades.

For the 8-point RFFT we choose 1, 1.5, 1, 0, 1, 1.5, 1, 0 as the input sequence. Because the RFFT architecture has 4 parallel inputs, the input sequence is injected to the systems in two stages. Concentrations for the inputs in the first and second stages and their corresponding outputs are tabulated in Table 1.

Table 1. Input and Output Order for the 8-Point RFFT Structure

stage	I1	I2	I3	I4	O1	O2	O3	O4
first	1	1.5	1	0	7	1	0	0
second	1	1.5	1	0	0	3	0	0

Figures 19 and 20 show the simulation results for the synchronous and asynchronous RFFT circuits, respectively. Table 2 compares the simulation results of the three operations, namely, the moving-average filter, the biquad filter, and the RFFT transform, in both the synchronous and asynchronous frameworks. The error in this table is computed as the difference between the output value obtained by simulation, O_s, and the theoretical output, O_t. On the one hand, Table 2 shows that the synchronous scheme has lower error. On the other hand, it is much slower than the asynchronous scheme.

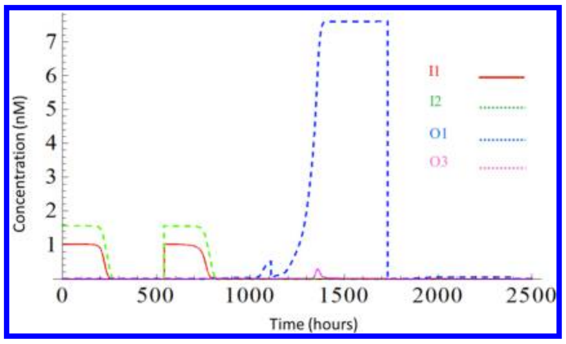

Figure 19. Simulation results for DNA implementation of the synchronous 8-point RFFT.

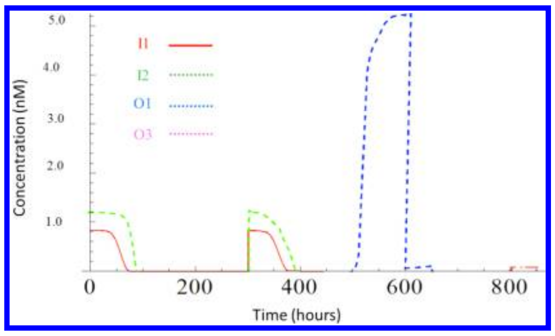

Figure 20. Simulation results for the DNA implementation of the asynchronous 8-point RFFT.

Table 2. Comparison for Moving-Average, Biquad, and FFT Designs, Synchronous and Asynchronous

system	scheme	no. of reactants	no. of reactions	calculation time (h)	% error ($\left\|\frac{O_s - O_t}{O_t}\right\| \times 100$)
moving average	synchronous	22	29	80	4.21
	asynchronous	16	24	20	5.67
biquad	synchronous	37	44	80	8.63
	asynchronous	32	46	50	12.79
RFFT	synchronous	119	202	900	7.8
	asynchronous	213	225	425	22

■ CONCLUSION

There is a rich body of research discussing the implementation of computation and logical functions with genetic regulatory elements,[9−14] and yet, despite concerted efforts by the synthetic biology community, progress in the design of genetic circuits seem to have stalled at the level of circuits with perhaps 7−15 components. *In vivo* engineering of such circuits is hard work, fraught with experimental difficulties.

In contrast, *in vitro* molecular computation with DNA strand displacement is following a Moore's Law-like trajectory in the scaling of its complexity.[15] Indeed, Erik Winfree, Lulu Qian, and their students at Caltech can routinely go from a design of a DNA circuit with several hundred components to experimental validation of it in a matter of weeks.

One of the great successes of electronic circuit design has been in abstracting and scaling the design problem. The physical behavior of transistors is understood in terms of differential equations, say, with models found in tools such as SPICE.[16] However, the design of circuits occurs at more abstract levels, in terms of switches, gates, and modules.

Research in molecular computation could benefit from this hierarchical approach.

Although pertaining to biology, the contributions of this paper are not experimental nor empirical; rather they are constructive and conceptual. We have presented two general methodologies for implementing signal processing with molecular reactions. One of our methodologies uses *clocking* to implement *synchronous* computation. The other one is *self-timed* and *asynchronous*. In both cases, the computation itself is essentially *rate-independent*, meaning that within a broad range of values for the rate constants, the computation is exact and independent of the specific rates.

Certainly, engineering complex new reaction mechanisms in any experimental domain is a formidable task; for *in vivo* systems, there are likely to be many experimental constraints on the choice of reactions. However, the techniques that we have presented here are robust and scalable. Tackling general problems in molecular computation this way could be transformative for applications such as drug delivery and metabolic engineering.

AUTHOR INFORMATION

Corresponding Author

*E-mail: mriedel@umn.edu.

Notes

The authors declare no competing financial interest.

ACKNOWLEDGMENTS

This research is supported, in parts, by the NSF CAREER Award 0845650, NSF CCF 0946601, and NSF CCF 1117168.

REFERENCES

(1) Anderson, J. C., Clarke, E. J., Arkin, A. P., and Voigt, C. A. (2006) Environmentally controlled invasion of cancer cells by engineered bacteria. *J. Mol. Biol. 355*, 619−627.

(2) Venkataramana, S., Dirks, R. M., Ueda, C. T., and Pierce, N. A. (2010) Selective cell death mediated by small conditional RNAs. *Proc. Natl. Acad. Sci. U.S.A. 107*, 16777−16782.

(3) Zhang, D. Y., and Winfree, E. (2009) Control of DNA strand displacement kinetics using toehold exchange. *J. Am. Chem. Soc. 131*, 17303−17314.

(4) Soloveichik, D., Seelig, G., and Winfree, E. (2010) DNA as a universal substrate for chemical kinetics. *Proc. Natl. Acad. Sci. U.S.A. 107*, 5393−5398.

(5) Parhi, K. K. (1999) *VLSI Digital Signal Processing Systems*, John Wiley & Sons, New York.

(6) Epstein, I. R., and Pojman, J. A. (1998) *An Introduction to Nonlinear Chemical Dynamics: Oscillations, Waves, Patterns, and Chaos*, Oxford University Press, Oxford, U.K..

(7) Kepper, P. D., Epstein, I. R., and Kustin, K. (2008) A systematically designed homogeneous oscillating reaction: the arsenite-iodate-chlorite system. *J. Am. Chem. Soc. 103*, 2133−2134.

(8) Oppenheim, A., Schafer, R., and Buck, J. (1999) *Discrete-Time Signal Processing*, Prentice-Hall, Upper Saddle River, NJ.

(9) Gardner, T. S., Cantor, C. R., and Collins, J. J. (2000) Construction of a genetic toggle switch in Escherichia coli. *Nature 403*, 339−342.

(10) Weiss, R., Basu, S., Hooshangi, S., Kalmbach, A., Karig, D., Mehreja, R., and Netravali, I. (2003) Genetic circuit building blocks for cellular computation, communications, and signal processing. *Nat. Comput. 2*, 47−84.

(11) Beneson, Y., Gil, B., Ben-Dor, U., Adar, R., and Shapiro, E. (2004) An autonomous molecular computer for logical control of gene expression. *Nature 429*, 423−429.

(12) Endy, D. (2005) Foundations for engineering biology. *Nature 438*, 449−453.

(13) Ramalingam, K., Tomshine, J. R., Maynard, J. A., and Kaznessis, Y. N. (2009) Forward engineering of synthetic bio-logical AND gates. *Biochem. Eng. J. 47*, 38−47.

(14) Tamsir, A., Tabor, J. J., and Voigt, C. A. (2011) Robust multicellular computing using genetically encoded NOR gates and chemical 'wires'. *Nature 469*, 212−215.

(15) Qian, L., and Winfree, E. (2011) Scaling up digital circuit computation with DNA strand displacement Cascades. *Science 332*, 1196−1201.

(16) Nagel, L., and Pederson, D. (1973) *SPICE (Simulation Program with Integrated Circuit Emphasis)*, University of California, Berkeley, Berkeley, CA, Memorandum ERL-M 382.